ROBUST AUTOPILOT DESIGN FOR A HIGH-AGILE GROUND-TO-AIR MISSILE

Berno J.E. Misgeld, Raimund Dold, Thomas Kuhn and Harald Buschek
Diehl-BGT-Defence
Alte Nußdorfer Straße 13
88662 Überlingen
GERMANY
e-mail: berno.misgeld@diehl-bgt-defence.de

ABSTRACT

In this study a robust autopilot is designed for a surface launched air defence missile, which is currently developed by Diehl-BGT-Defence. The surface launched version is a further development of an existing high-agile thrust vector controlled missile, with satellite aided navigation midcourse guidance phase, infrared seeker, enhanced motor and flight envelope. The missile is developed as an air-defence weapon.
In order to cope with the highly nonlinear and time-varying dynamics and the extended flight envelope, a robust autopilot is designed using H_∞-optimal control and µ-synthesis. The control synthesis is accomplished for the lateral channel by using linearised models of the airframe, control actuation system and body bending, containing real uncertainty corresponding to the current flight condition. The flight controllers for lateral dynamics are designed for a number of different flight conditions and implemented using a combined blending/gain scheduling approach to cover nonlinearities, which depend on air speed and air density. The controllers are designed as single-input-single-output controllers and extended by an anti-windup scheme to handle actuator saturation. Aerodynamic coupling effects are reduced significantly by a manoeuvre-plane roll control bank-to-turn approach, in an initial turn and end-game manoeuvre. The flight control laws are extended by a roll-decoupling for lateral channels and tested in a high-fidelity six degrees-of-freedom model using full aerodynamics and uncertainty offsets. The superior performance and robustness characteristics are demonstrated in extreme flight manoeuvres, as to be proven in upcoming flight tests.

1. INTRODUCTION

Automatic flight control systems for modern missiles have to cover a wide operating range, depending on the flight envelope and the agility of the missile. In order to guarantee feedback control properties like fast and accurate reference tracking while maintaining high rate damping and stability, the modern missile autopilot has to be designed for a highly nonlinear and time-variant system.
With the introduction of classical gain scheduling controllers during the last century many critical issues in autopilot design were successfully solved for most missiles [1],[2]. Such difficulties are for example system inherent nonlinearities depending on incidence angle or airspeed, coupling effects in the multivariable feedback control system, time-varying effects like motor burn time dependent inertia and mass properties. For the design of modern missiles, the extended flight and manoeuvre envelope leads to gain scheduling control systems which are difficult to tune because of a rising number of controllers, that is the number of interpolation points. This leads, unless an automation of controller tuning is possible, to an expensive missile autopilot design. Furthermore, uncertainties that exist at linear controller tuning points cannot be taken explicitly into the design procedure.
The development of robust control techniques during the 1980's has given the possibility to include uncertainties and a number of control design requirements to the controller design. Methods like H_∞ design and µ-synthesis provide a multivariable control design framework to include frequency dependent control weightings as well as real and complex uncertainty. The application of these methods showed promising results when applied to missile autopilots ([3], [4], [5], [6]). An application of a robust controller to the high-agile air-to-air missile, developed by Diehl BGT Defence, was presented in [7]. The controller was implemented via a blending/conditioning approach depending on dynamic pressure and showed superior performance in flight tests [8]. In this paper, a lateral robust autopilot is developed using the µ-synthesis method for a surface launched ground-to-air missile. This autopilot is based on the robust autopilot of [7], but is extended and re-designed to cope with the larger flight envelope. The missile is a four wing axis-symmetric thrust vector controlled missile with radio uplink and satellite aided navigation. The missile distinguishes three distinct phases of flight, which are initial turn, mid-course and end-game. During initial turn and end-game the missile is steered in a bank-to-turn manoeuvre plane approach for high incidence angle in missile main axis configuration. By using combined aerodynamic and thrust vector control, the missile is designed to engage highly agile manoeuvring targets with a considerable amount of lateral acceleration. In this paper the autopilot for lateral channels is presented, which is designed for rapidly changing (time-varying), highly nonlinear dynamics.
This paper is organised as follows. Chapter 2 describes the system modelled for controller synthesis. In Chapter 3 the controller synthesis is presented. The extended roll decoupling and scheduling/blending design is given in Chapter 4. Nonlinear simulation results are shown in Chapter 5. Finally this paper ends with a discussion of the results.

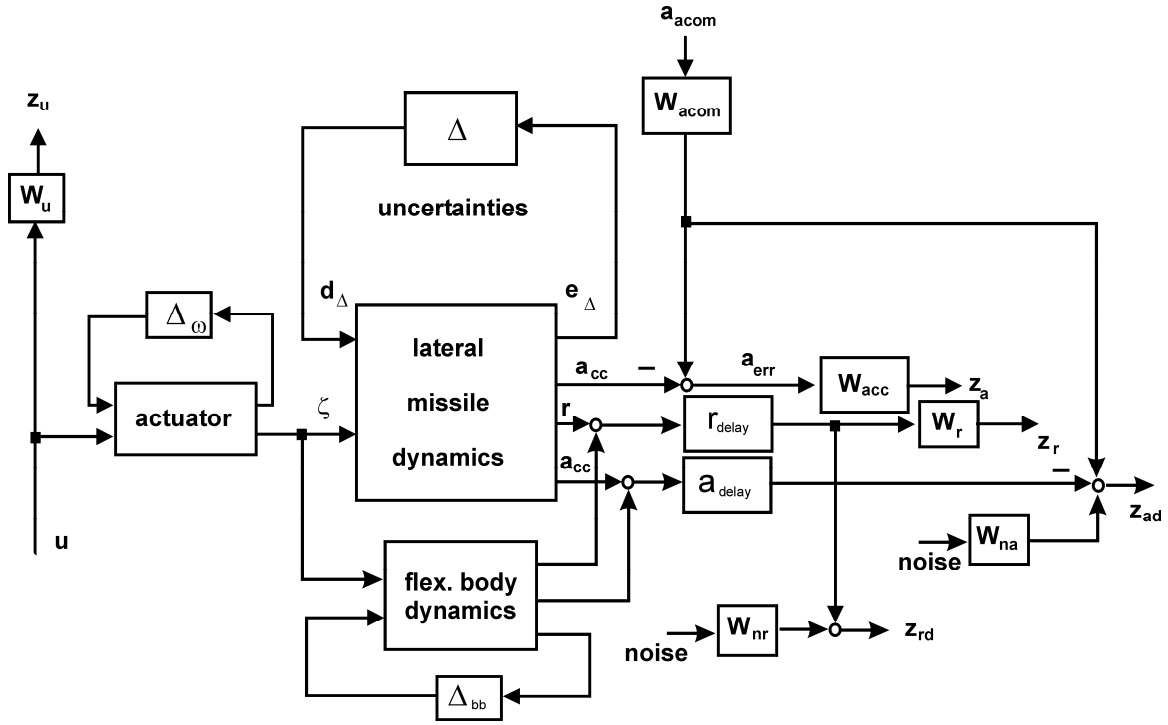

FIG 1. Plant interconnection structure for controller synthesis

2. SYSTEM MODELLING

The nonlinear missile dynamics are linearised at a number of certain operating points, where speed (Mach number) is the main nonlinearity. The linear six-degrees of freedom model is decoupled into pitch, yaw and roll motion for single-input single output (SISO) controller design. Uncertainties depending on mass or inertia properties, thrust vector control and incidence angle are modelled into the parameters of the linear equations. Since the dynamic behaviour in both lateral channels is equal, an autopilot is designed for lateral and roll channel. The linearised lateral dynamics are used for controller design, FIG 1, and can be described by a second order state space model

$$\frac{d}{dt}\begin{bmatrix} r \\ \beta \end{bmatrix} = \begin{bmatrix} N_r & N_\beta \\ -1 & \frac{Y_\beta}{V_0} \end{bmatrix}\begin{bmatrix} r \\ \beta \end{bmatrix} + \begin{bmatrix} N_\zeta - c_{th}\frac{l_{th}T}{I_{zz}} \\ \frac{Y_\zeta}{V_0} - c_{th}\frac{T}{mV_0} \end{bmatrix}\zeta$$

$$\begin{bmatrix} r \\ a_{y,CG} \\ a_{y,IMU} \end{bmatrix} = \begin{bmatrix} 1 & 0 \\ 0 & Y_\beta \\ l_{acc}N_r & Y_\beta + l_{acc}N_\beta \end{bmatrix}\begin{bmatrix} r \\ \beta \end{bmatrix} + \begin{bmatrix} 0 \\ Y_\zeta + c_{th}\frac{T}{m} \\ Y_\zeta + l_{acc}N_\zeta + c_{th}\left(\frac{T}{m} - l_{acc}\frac{l_{th}T}{m}\right) \end{bmatrix}\zeta \quad (1)$$

where β is the sideslip angle, r is the yaw rate and the input to the equations is ζ the rudder deflection. Output of the equations are yaw rate r, centre of gravity acceleration $a_{y,CG}$ and inertial measurement unit acceleration $a_{y,IMU}$. The thrust vector control effects are modelled in the input vector of (1), where T is the thrust, l_{th} is the distance between centre of gravity and the nozzle and the factor c_{th} relates the fin deflection angle to the actual thrust vector deflection. In addition to the time-varying effects of the thrust vector control, equations (1) depend on the effect of mass m, moment of inertia I_{zz} and lever arm l_{acc} (centre of gravity to IMU position).

The derivatives of (1) depend on the operating point, which is incidence angle, airspeed and dynamic pressure, and can be given by [12]

$$\begin{aligned} N_\beta &= \bar{q}\frac{Sl_r}{I_{zz}}C_{n\beta} \\ N_r &= \bar{q}\frac{Sl_r}{I_{zz}}\frac{l_r}{V_0}(C_{nr} + C_{n\dot{\beta}}) \\ N_\zeta &= \bar{q}\frac{Sl_r}{I_{zz}}C_{n\zeta} \\ Y_\beta &= \bar{q}\frac{S}{mV_0}(C_{Y\beta} - C_W) \\ Y_\zeta &= \bar{q}\frac{S}{mV_0}C_{Y\zeta} \end{aligned} \quad (2)$$

Note that, for controller design the time dependency of equations (1) and (2) is neglected and modelled as

uncertainty in terms of burn time effects. The controllers are designed at certain speed operating points and at sea level altitude. Effects of incidence (side-slip) angle and total control deflection are taken into account as uncertainties for design. Uncertainties for each state space matrix element were determined using a trim routine, where derivative data is collected at each valid trim point incidence angle, neighbouring Mach range, thrust vector control and varying mass and inertia. This is done by an automatic trim routine, which reconfigures the data for an adequate uncertainty representation by a mean value and respective percentage uncertainty.
For controller design the model of (1) is extended by a model of the structural vibrations (body bending). Only the first bending mode is modelled using a low damped oscillator state space model of second order

$$\begin{bmatrix}\dot{x}_{bb,1}\\ \dot{x}_{bb,2}\end{bmatrix}=\begin{bmatrix}0 & 1\\ -\omega_{bb}^{\ 2} & -2\zeta_{bb}\omega_{bb}\end{bmatrix}+\begin{bmatrix}0\\ 1\end{bmatrix}\zeta$$
$$\begin{bmatrix}\Delta r\\ \Delta a_{y,CG}\\ \Delta a_{y,IMU}\end{bmatrix}=\begin{bmatrix}0 & k_{q,bb}\\ -k_{a,bb}\omega_{bb}^{\ 2} & -2k_{a,bb}\zeta_{bb}\omega_{bb}\\ -k_{a,bb}\omega_{bb}^{\ 2} & -2k_{a,bb}\omega_{bb}\zeta_{bb}\end{bmatrix}\begin{bmatrix}x_{bb,1}\\ x_{bb,2}\end{bmatrix}+\begin{bmatrix}0\\ k_{a,bb}\\ k_{a,bb}\end{bmatrix}\zeta \quad (3)$$

in which ω_{bb} and ζ_{bb} are the body bending frequency and the damping. The input ζ is the rudder command, calculated from fin deflections and the outputs are the delta rates and accelerations, applied by addition to equation (1). $k_{a,bb}$ and $k_{q,bb}$ are the rate and acceleration gains, calculated from constants, derived by a mechanical finite element model and validated by body bending tests [7]. The rudder deflection ζ is the command signal, given by the autopilot and realised by the control actuation system (CAS). The CAS dynamics for autopilot design were modelled in a simplified second order model with damping and resonance frequency, where uncertainties were included to the damping of the CAS. Finally, the time-delay of the flight computer was model as two sample time instances, with a continuous first order Padé approximation to

$$G_{r,a}(s)=\frac{-\frac{n_d s}{T_s}+2}{\frac{n_d s}{T_s}+2}, \quad (4)$$

where T_s is the system sampling time, n_d =2 is the assumed time delay. Equation (4) is applied to the outputs of (1).

3. CONTROL SYNTHESIS

3.1. Controller interconnection and uncertainty modelling

For the controller design, the model consisting of equations (1) to (3) is extended with the control actuation system and interconnected with diagonal block uncertainty (real) and complex weighting functions, FIG 1. The controller design for the lateral controller is conducted as a (1, 2) controller consisting of a rate damper in feedback configuration in the inner-loop and an acceleration command tracking controller in the outer loop. The controller output is the CAS input signal, which is extended by a complex weighting to limit the actuation bandwidth

$$W_u(s)=\frac{k_u(z_u s+1)}{p_u s+1}, \quad (5)$$

where k_u is the static gain, z_u is zero and p_u is the pole inverse of the transfer function. The parameters are determined from given crossover frequency and gain at high/low frequencies. Weightings on yaw rate and acceleration sensitivity functions are introduced to specify the damping of the rate circuit and the tracking performance of the acceleration loop, where W_r is modelled as a static gain and $W_{acc}(s)$ is given by

$$W_{acc}(s)=\frac{k_{acc}(z_{acc}s+1)}{p_{acc}s+1}. \quad (6)$$

In (6) the parameters k_{acc}, z_{acc} and p_{acc} are again derived from gain at low frequencies (steady state error for the acceleration loop), crossover frequency and high frequency gain. Note that (6) does not have integral action, which means that the outer-loop acceleration tracking circuit does not have any integral action. This is done do get better stability properties in the outer-loop. W_{acom} is a weight for the reference tracking loop, which is chosen as a constant factor to specify the ratio of acceleration tracking loop to rate damping loop. The feedback channels of rate and acceleration are corrupted by measurement noise, which is modelled in the weighting

$$W_{na}=k_{na}, \qquad W_{nr}=k_{nr}. \quad (7)$$

The measurement noise weightings are not frequency dependent. In addition to the weightings, the models of the lateral dynamics, CAS and body bending are extended by uncertainties, represented by the structured (real) uncertainty block

$$\Delta=\begin{bmatrix}\delta_\beta & & & \\ & \delta_\zeta & & \\ & & \ddots & \\ & & & \delta_{bb}\end{bmatrix}, \quad (8)$$

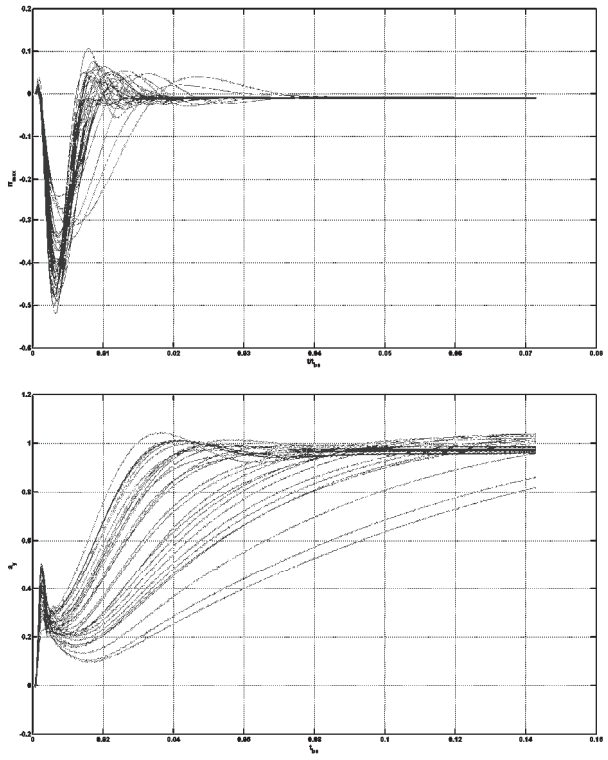

FIG 2. Step responses of inner-loop compensator (upper) and outer-loop acceleration circuit (lower) with full modelled uncertainty.

where $\delta_\beta, \delta_\zeta, \ldots \delta_{bb}$ are real scalar perturbations $-1 \le \delta_i \le 1$ and correspond to the uncertainties in the state-space parameters in (1) to (3) and the CAS. For controller synthesis, the plant is brought to the general control configuration [9], [13], with the block diagonal matrix (8).

3.2. Controller μ-synthesis

Using the interconnection structure given in FIG 1 the lateral controllers were designed at five different Mach numbers using the μ-synthesis via DK-iteration. The performance functions (5)-(7) were determined for each single controller synthesis point to optimise the trade-off between controller robustness properties, noise rejection and controller performance specification. Controller tuning was conducted with full airframe uncertainty at the current operating condition, which means over full incidence models, control effectiveness, thrust vector control and mass/inertia. It turns out, however, that the controllers are of high order and tend to be too conservative, resulting in higher μ-values for robust stability and robust performance. Furthermore, the low damped body bending leads to numerical problems, depending on complex performance weightings and design points. Therefore, the uncertainty modelling and controller design was rearranged.

The nominal values for lateral uncertainties were set to minimum incidence values. The space of uncertainties was significantly reduced to ±30% - ±70%, depending on the value of lateral dynamics. The structural vibration model (3) was removed from the controller synthesis model to avoid numerical problems in the controller synthesis. To damp the body bending after controller synthesis a notch filter was applied to the measurement signals after controller tuning. The controller synthesis was conducted using the following automated design procedure:

1) Determine design weightings and uncertainties dependent on Mach design point and interconnect model for controller μ-synthesis.
2) Conduct controller μ-synthesis via DK-iteration with performance model.
3) Reduce controller to 7th-order via balanced realisation [10].
4) Check time-domain response of lateral dynamics using the full uncertainty model with signal conditioning (notch filter) and the 7th-order reduced controller.
5) Determine robust stability via μ-analysis using the full airframe, body bending and CAS uncertainty with applied time-delay on output and signal filtering and conditioning.
6) Determine robust performance via μ-analysis using the full uncertainty model with body bending and signal filtering.

Depending on time-response properties (damping, settling time and steady-state error) and structured singular values for robust stability and performance the controllers were chosen for further tests in the 6DOF model or re-tuned in the automated procedure. The result are controllers which lead to lower structured singular values and a better control performance. FIG 2 shows an example of the linear controller response in time-domain using the model with full uncertainty. Note that mainly the large variation in control effectiveness leads to the broad range of responses, which can be reduced significantly by a higher gain controller. An example of the structured singular values, achieved in inner- and outer-loop is given in FIG 3. Over all calculated frequencies, the value of

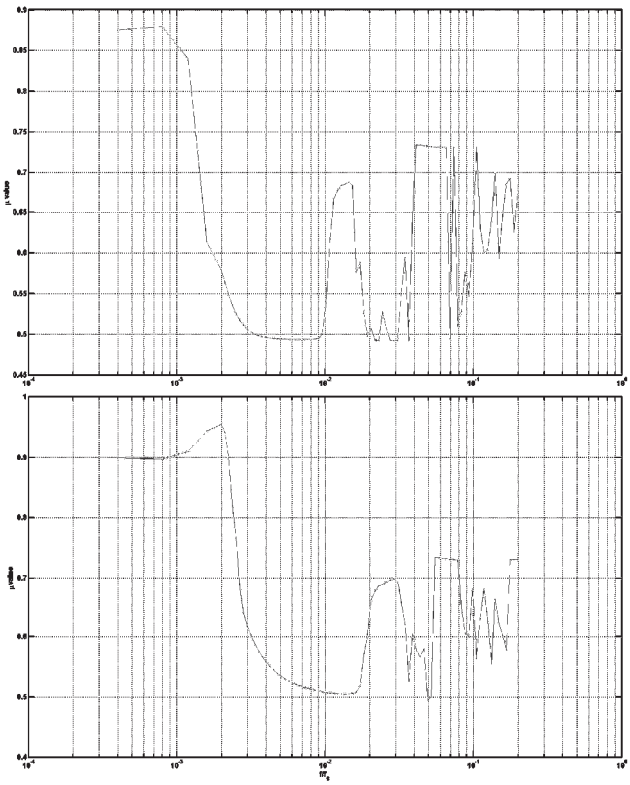

FIG 3. Structured singular value for robust stability with full uncertainty inner-loop (upper) and outer-loop (lower) part of the figure.

structured singular value μ does not reach one, meaning the controller can tolerate over 100% of the modelled uncertainties. Similar results as shown in FIG 3 were achieved with the other controllers in SISO robustness analysis.

4. AUTOPILOT GAIN SCHEDULING AND IMPLEMENTATION ISSUES

Five lateral flight controllers were designed for the complete speed envelope of the missile. Each of the controllers covers a certain speed region of the missile for sea level altitude. Since the process dynamics of the missile are significantly dependent on altitude, namely air density, the lateral autopilot was scheduled on altitude

$$k_{lat} = \frac{\rho}{\rho_0}, \tag{9}$$

where ρ is the current air density and ρ_0 is the sea level air density. The lateral gain k_{lat} is applied to the rate channel and the acceleration channel. This is a valid scheduling approach, since each entry of the linearised plant dynamics is dependent on the air density. This does not hold for the thrust vector control of (1). However, it turned out in simulations that the influence of thrust vector control variation does not lead to a destabilisation of the lateral control system with altitude scheduling when applied to nonlinear simulations.

Blending and anti-windup of the controllers are realised by using a combined blending anti-windup scheme, presented in [7][11] as the “high gain anti-windup approach”. The Mach number is used as the blending variable and the controllers are blended in a smooth transition phase using high-feedback gain. In this approach the controllers are slowly switched on by using the percentage value the controller is to be used, to reduce the controller input error signal. If a relatively slow blending phase and variable (compared to controller dynamics) can be guaranteed, this approach works well for the overall flight envelope.

To reduce the effect of high roll rate manoeuvres, the lateral autopilot is implemented in a de-rolled lateral frame. For that, a transformation is applied to lateral acceleration errors and rates at the input of the controller and at the rudder command at the output. For example, measured pitch and yaw rate input to the controller are transformed as

$$\begin{bmatrix} q \\ r \end{bmatrix}_d = \begin{bmatrix} \cos\phi_b & -\sin\phi_b \\ \sin\phi_b & \sin\phi_b \end{bmatrix} \begin{bmatrix} q \\ r \end{bmatrix}_{meas}, \tag{10}$$

with ϕ_b, the body roll angle, integral of the roll rate. This transformation decouples the lateral integrator-like states from roll motion on high roll rates, leading to better performance even with higher sampling times of the overall flight computer.

The missile roll control uses a bank-to-turn manoeuvre plane logic for initial turn and end-game manoeuvres and a skid-to-turn roll autopilot for satellite aided mid-course phase of flight. The initial turn and end-game roll autopilot

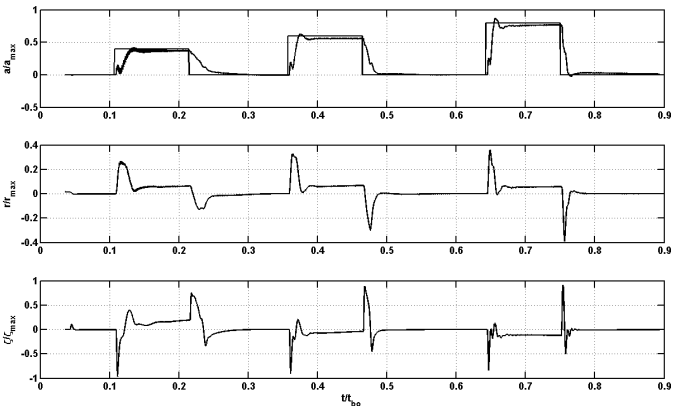

FIG 4. Acceleration reference steps and IMU response during motor burn phase, sea level altitude (6DOF

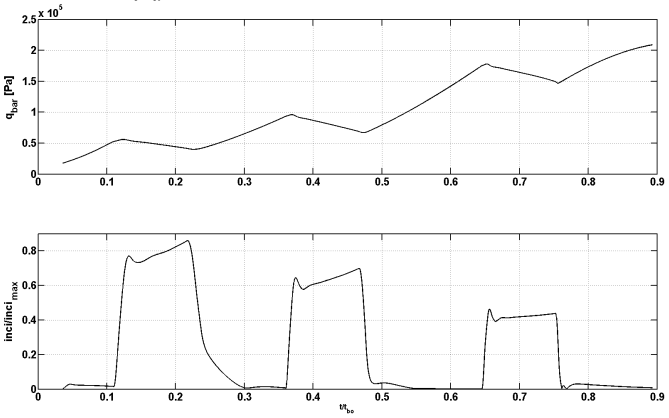

FIG 5. Dynamic pressure and incidence angle during acceleration reference steps, sea level altitude (6DOF model).

has to guarantee main manoeuvre plane bank-to-turn behaviour even with high-agile manoeuvring targets. This is achieved by a sophisticated manoeuvre plane logic and a high gain roll autopilot. An acceleration limiter, depending on speed, altitude and manoeuvre plane angle is used to limit the guidance acceleration commands to remain in trimmable flight conditions. Off-plane mixed axis flight control acceleration commands are simulated in a 6DOF environment (without manoeuvre plane logic) to ensure the robust behaviour of the multivariable system.

5. NONLINEAR SIMULATION

Nonlinear simulations were conducted in a Matlab/Simulink 6-degrees-of-freedom model, to validate controller performance and robustness in a first step. The model contained full aerodynamics (wind tunnel data) and thrust vector control, coupled 6DOF equations of motion, nonlinear structural vibration, a simplified motor model, atmosphere and the full operational three axis autopilot. Tests with the controller were conducted over the whole flight envelope for reference tracking and disturbance rejection. FIG 4 shows example acceleration reference steps during motor burn phase, with the corresponding dynamic pressure and the incidence angle given in FIG 5. Note that acceleration steps are scaled with the structural acceleration limit, the rate and rudder commands are scaled by the maximum allowable rate and rudder command limit. The overall response during varying speed, resulting in a rising dynamic pressure during motor burning is fast, due to controller blending. The overshoot

during these acceleration tracking response tests remained below 10%, the steady-state error is relatively low. Incidence angles, necessary to realise the commanded acceleration can be seen in the lower part of FIG 5. Depending on dynamic pressure and missile speed, the incidence angle varies from 40% to 90% of the allowable maximum incidence limit. Reference step tests were applied during motor burn phase, burn out and at different altitudes and missile speed, in which similar results to FIG 4 were achieved with the coupled system. For these tests, the model in MATLAB/Simulink was initialised with speed, altitude and at different motor burn times. In addition to the reference tracking tests in single axis configuration, reference steps were applied to both lateral channels. In this case the command limitation has to be regarded in terms of a trimmable airframe. FIG 6 shows an example of acceleration reference steps in both channels, during burn-out phase of flight (transonic to subsonic). After a fast transient response, a steady-state error can be seen, which is reduced after a short time period. The response of the rates (FIG 6, (b)) is damped and the incidence angle is at 60% of the allowable value. Note that this condition is not allowed to occur in initial turn or end-game condition, where the manoeuvre plane control is active. During skid-to-turn mid-course phase mixed lateral command signals can occur, but are limited via an acceleration limiter depending on the aerodynamic roll angle.

After successful test of the lateral controllers in the MATLAB/Simulink model, the autopilot was implemented in a validated simulation model of the missile. In addition to the nonlinear 6DOF equations of motion and wind tunnel aerodynamics, this model contained a detailed motor section, control actuator system and sensor (accelerometer and gyros) model. Controller rate and acceleration input signals are corrupted by sensor, motor and airframe noise, which were implemented according to real flight data measurement. The controllers were implemented in the operational flight software and control response tests were conducted over a whole single mission, for upcoming flight tests. Acceleration reference steps were applied to the system with no guidance loop and are shown in FIG 7. The ramp like first reference step corresponds to the acceleration reference limiter at beginning flight condition and low speed of the missile. Reference steps applied to both channels show fast dynamic behaviour with small steady state errors of below 10% and in most cases below 5%. No overshoot can be seen over the whole flight, meaning at different blending phases of the lateral controllers. Test were repeated with a varying level of acceleration steps and similar good results were obtained, where in some cases slight overshoots corresponding to the results, shown in FIG 7 can be seen.

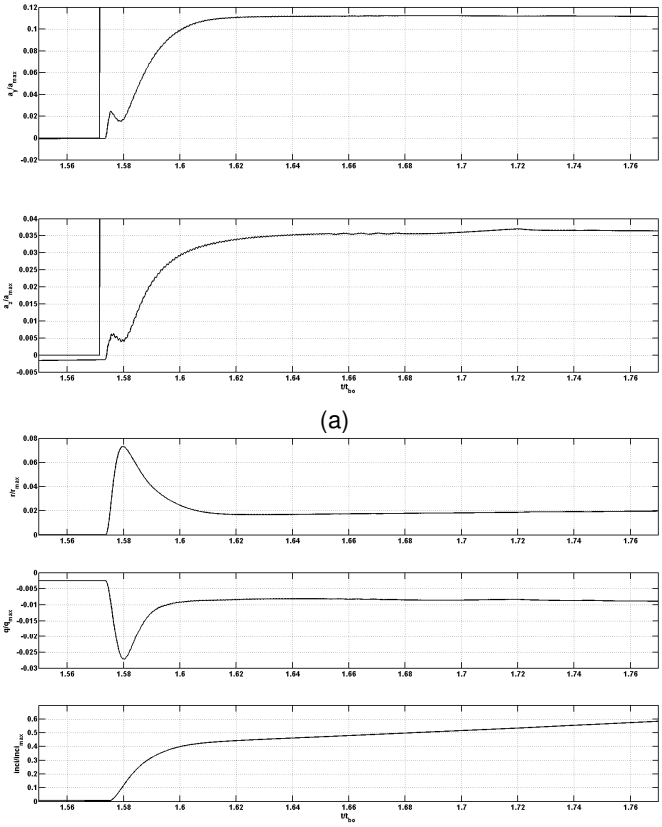

(a)

(b)

FIG 6. Acceleration loop response (IMU) to an acceleration reference step-like change in y- and z-body axis during burn-out phase of flight (a). Corresponding normalised rates and incidence angle (b).

6. RESULTS AND DISCUSSION

A robust autopilot design for a high-agile ground-to-air missile was presented. Following the linearisation of the airframe at certain trim conditions, a linear model was used for controller design. The model contained full uncertainties at a single flight condition, described by Mach number and sea level altitude. The uncertain lateral dynamics were extended by CAS, time-delay and body bending effects. For μ-synthesis controller design using DK-iteration, the uncertain plant was extended by performance weightings and process noise. The results of the controller tuning process are conservative high-order controllers, which were difficult to reduce in order because of numerical problems. The controllers did not achieve satisfying structured singular values for robust stability or control performance, which is related to the large plant uncertainty and the body bending effects. Therefore, the uncertainties of the plant were reduced significantly and structural vibrations were removed from the design model. The controllers were designed with a new design model, where signal conditioning and filtering of the measurement signals was applied to the control feedback after controller tuning. The controllers tuned with the second lateral design approach lead to much better structured singular values and can tolerate uncertainties of more than 100% in acceleration and damping loop with the model of full uncertainty and body bending. Since the tuning procedure is more time consuming due to the robust stability and robust performance checks, the approach was automated. Five controllers were tuned for the lateral channels and the complete flight envelope at lea level and varying Mach numbers. For nonlinear simulation the lateral controllers were implemented with the high-gain feedback blending approach and gain scheduled with the inverse of the normalised air density to compensate loop gain at higher altitudes. The gain scheduling/blending approach was not part of the robustness analysis, as well as the multivariable control system behaviour. Multivariable control-loop behaviour and the gain scheduling blending approach were tested in nonlinear simulations. Step-response tests were processed at single operating points using a MATLAB/Simulink model with the three axis autopilot. Good control performance was achieved over the whole

flight envelope and at different motor burn times. A slight tendency to overshoots of less than 10% was observed with thrust vector control support and at larger altitudes. This effect can be addressed to the gain scheduling in dependence of altitude and thrust vector effects. In a second validation step, the lateral controllers were implemented in the operational flight computer and tested in reference control tracking tests using a validated model of the missile. Extensive test series at varying acceleration reference levels and with different flight profiles underline the good control loop and damping results obtained with the MATLAB/Simulink model. The control response test results of the multivariable control loop did not degrade in high-incidence angle manoeuvres. A degrading effect of the combined blending/gain scheduling approach on stability could not be seen during nonlinear simulations. Since the robustness of the multivariable control loop cannot be quantified in simulations, a multivariable robustness analysis including controller conditioning/blending effects will be subject to future work. Currently, the controllers are prepared for Monte-Carlo control response simulation tests with random uncertainties, which are performed for controller validation for upcoming real world flight tests.

7. LITERATURE

[1] Nesline, F.W. and Zarchan, P.: "Robust Instrumentation Configurations for Homing Missile Flight Control", *Proceedings of the AIAA Guidance, Navigation, and Control Conference*, Danvers, MA, Aug. 1980, pp. 209-219

[2] Rugh, W.J. and Shamma, J.S.: "Research on gain scheduling", Automatica, 36, pp. 1401-1425, 2000

[3] Reichert, R. T.: Application of H_∞ Control to Missile Autopilot Design, AIAA Guidance, Navigation and Control Conference, Boston, MA, pp. 1065-1072, 1989

[4] Wise, K.A., Mears, B.C. and Poolla, K.: "Missile Autopilot Design Using H_∞ Optimal Control With μ-Synthesis", *Proceedings of the American Control Conference*, San Diego, CA, 1990, pp. 2363-2367

[5] Yang, S.M. and Huang, N.H.: "Application of H_∞ Control to Pitch Autopilot of Missiles", *IEEE Transactions on Aerospace and Electronic Systems*, Vol. 32, No. 1, Jan. 1996, pp. 426-433

[6] Jackson, P.: "Applying μ-Synthesis to Missile Autopilot Design", *Proceedings of the 29th IEEE Conference on Decision and Control*, Honolulu, HI, 1990, pp. 2993-2998

[7] Buschek, H.: Full Envelope Missile Autopilot Design Using Gain Scheduled Robust Control, Journal of Guidance, Control and Dynamics, 22(1), pp. 115-122, 1999

[8] Dold, R. and Buschek, H.: "Flight Test of a Scheduled μ-Synthesis Autopilot for an Air-To-Air Missile", AIAA Guidance, Navigation and Control Conference, Montreal, Canada, 2001

[9] Skogestad, S. and Postlethwaite, I.: Multivariable Feedback Control, John Wiley and Sons, Chichester, 2005

[10] Chiang, R.Y. and Safonov, M.G.: „Robust Control Toolbox, User's Guide", The MathWorks Inc., Natick, MA, Aug. 1992

[11] Hyde, R. A.: H_∞ Aerospace Control Design, Springer-Verlag Berlin Heidelberg New York, 1995

[12] Stevens, B. L. and Lewis, F. L.: Aircraft Control and Simulation, John Wiley and Sons, New Jersey, 2003

[13] Zhou, K., Doyle, J., Glover, K.: Robust and Optimal Control, Prentice Hall, New Jersey, 1996

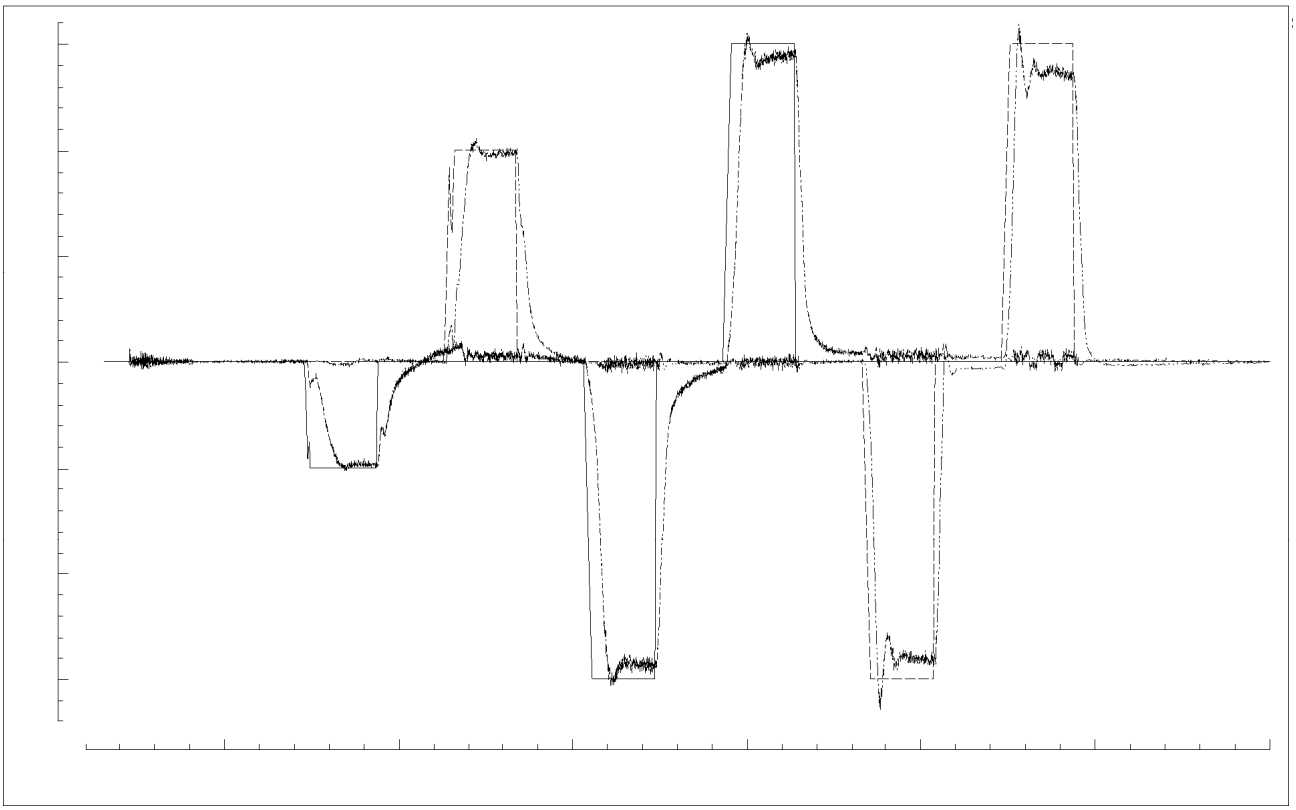

FIG 7. Lateral control response tests in two lateral channels with three axis autopilot during single mission.